THE ASTROPHYSICAL JOURNAL, ???: ??–??, 2003 MONTH, ASTRO-PH/YYMMNNN
Preprint typeset using LaTeX style emulateapj v. 4/9/03

TIME DELAY MEASUREMENT OF THE LENSED QUASAR HE1104−1805

ERAN O. OFEK AND DAN MAOZ
School of Physics and Astronomy, and Wise Observatory, Tel-Aviv University, Tel-Aviv 69978, Israel.
Received 2003 May 6; accepted 2003 May 9

ABSTRACT

We have measured the time delay between the two images of the gravitationally lensed quasar HE1104−1805 by combining observations made with the Wise Observatory 1m telescope and published observations of this system by Schechter et al., spanning a total of five years, from 1997 to 2002. Based on a variety of techniques, we find that the best fit time delay is $-161^{+7,+34}_{-7,-11}$ days. The 68% and 95% confidence intervals include the systematic errors due to an observed component of uncorrelated variability between images. The delay is shorter than predicted by simple models and may indicate a large external shear or a large value of the Hubble parameter, $h > 0.75$ (95% confidence). The residual light curve between the two images shows a longterm trend of ~ 0.04 mag yr^{-1}, presumably the result of microlensing by stars in the lens galaxy, but also short timescale (~ 1 month) variability with a mean amplitude of about 0.07 mag.

Subject headings: cosmology: gravitational lensing — Quasars: general — Quasars: individual (HE1104−1805)

1. INTRODUCTION

Time-delay measurements in a large sample of gravitationally lensed systems could be used to measure the Hubble parameter, H_0, directly at high redshift, therefore avoiding the systematics due to distance ladder calibrations and large-scale motions (e.g., Turner, Cen, & Ostriker 1992). Alternatively, using a measured value of the Hubble parameter from other techniques (e.g., Bennett et al. 2003), measurement of a time delay allows discriminating between different mass profiles of galaxies (e.g., Kochanek 2002). In some systems, complex geometries caused by multiple lensing galaxies hinder the use of time delay measurements for H_0 determination or for mass profile studies. Even in such systems, time delay measurements are important for isolating the microlensing variability from the intrinsic variability. Microlensing in lensed quasars could allow an independent measurement of the fraction of dark matter in galaxies (Schechter & Wambsganss 2002), and can be used to put limits on the size of the continuum emission regions in quasars (e.g., Wambsganss, Paczynski, & Schneider 1990; Wambsganss 2002; Wyithe, Agol, & Fluke 2002).

HE1104−1805 is a double-image lensed quasar discovered by Wisotzki et al. (1993). The image separation is $\Delta\theta = 3.19''$, the source redshift is $z_s = 2.319$ (Wisotzki et al. 1993), and the lens redshift is $z_l = 0.729$ (Lidman et al. 2000). This is an unusual system, in which the image closer to the lens (image *A*) is the brighter one. Wisotzki et al. (1993) noted the emission line flux ratio between the images is 2.8, and that component *A* has a bluer continuum and lower equivalent width emission lines than *B*. They interpreted the differences as being caused by microlensing of the quasar continuum source in the brighter image. Wisotzki et al. (1995) reported that the continuum flux in both images is highly variable, but that the line fluxes do not change. Again, this could be interpreted as evidence for strong microlensing. Lehár et al. (2000) have attempted modeling this system. They assumed an image flux ratio of about 4, and found this limits the models to a narrow range of predicted time delays.

Wisotzki et al. (1998) measured the continuum flux in 19 low resolution spectra, taken with the ESO 3.6m telescope between 1993 to 1998. By matching the light curves of the two images, they favored a time delay of about −270 days (in the sense that the *B* image leads the *A* image), although they concluded that a value as short as −100 days could not be excluded. Gil-Merino, Wisotzki, & Wambsganss (2002) analyzed the *B*-band acquisition frames for the spectroscopy of Wisotzki et al. (1998) and found a best fit time delay of -310 ± 20 days (2σ errors). Pelt, Refsdal, & Stabell (2002) re-analyzed the Gil-Merino et al. (2002) observations, and argued that the time delay is somewhere between −330 and −255 days, but with a large uncertainty. In a recent paper, Schechter et al. (2003) presented 3 years of *V*-band photometry of HE1104−1805, obtained on 102 nights with the OGLE 1.3m telescope. They did not succeed in finding a consistent time delay for the system. In fact, the root-mean-square (rms) of the difference between the component light curves as a function of time delay showed two minima, at about −150 days and −360 days. Moreover, Schechter et al. (2003) noted that the structure functions of images *A* and *B* are quite different, with image *A* being more than twice as variable as image *B* on timescales of less than a month. Thus, there is presently no clear evidence of a time delay in this system, let alone an unambiguous measurement of its value.

In this paper we present new photometric data for HE1104−1805 from the Wise Observatory lens monitoring project. Combined with the OGLE observations of HE1104−1805 from Schechter et al. (2003), our data establish the delay securely and isolate the various correlated and uncorrelated variability components. We will assume throughout a cosmology with $\Omega_m = 0.3$, $\Omega_\Lambda = 0.7$, and $H_0 = 100h$ km s^{-1} Mpc^{-1}.

2. OBSERVATIONS AND REDUCTION

For the past three years we have been monitoring a sample of 27 known gravitationally lensed quasars and lens candidates with the Wise Observatory 1m telescope. The objects are monitored on a weekly basis in the Johnson-Cousins *R*-band, with occasional coverage in the *I*-band or *V*-band. Frames are obtained with a cryogenically cooled Tektronix 1024×1024-pixel back-illuminated CCD. The scale is $0.7''$ per pixel. The median seeing of about $2''$ does not al-

Electronic address: eran@wise.tau.ac.il

low resolving most of the lensed objects. However, some of the pairs are resolved (e.g., Q0142−100, HE1104−1805, RXJ0921+4528, Q0957+561). The data are reduced automatically on a daily basis. In each field we perform aperture photometry of all sources in the frame and the preliminary combined-image light curves are posted on the WWW[1].

We present here *R*-band measurements of HE1104−1805 taken between 1999, November 14 and 2002, June 18. The combined OGLE and Wise observations span over five years, from 1997 to 2002. The Wise observatory photometry of HE1104−1805 was performed using a special program we have written for this purpose. All the frames are aligned and rotated to the same reference frame. The program constructs a numerical point-spread function (PSF) from preselected reference stars. Given accurate positions of the lensed images from Hubble Space Telescope images (Lehár et al. 2000), it fits the PSF to the images and minimizes the χ^2 (assuming Poisson noise) with respect to the two free parameters, the magnitude of the two images, m_1 and m_2. In the case of HE1104−1805, the PSF was constructed from 12 stars. After rejecting all measurements with errors larger than 0.1 mag, we are left with 79 epochs for image *A* and 49 epochs for image *B*[2]. Note that the light contributed by the lensing galaxy to image *A* was neglected in the photometry, as it contributes only 0.3% and 3.5% of the total light of image *A* in the *V* and *I* bands, respectively.

The error bars were calculated from the covariance matrix of the χ^2 surface (e.g., Press et al. 1992). To validate the reliability of the error bars, we have made an empirical, magnitude dependent, error estimate for each lensed image and compared it with the χ^2 error estimate. The empirical errors were calculated as follows. Using the same algorithm, we have measured the difference, Δm_i^t, for each frame taken at epoch t, between the magnitude of each reference star, i, and its average magnitude over time, $\bar{m}_i$ (with the magnitudes measured relative to the 12 co-added reference stars). The error in the measurement of a particular source will depend on its intrinsic magnitude and on the observing conditions on the particular epoch. To find this dependence, we fit a function, with two free parameters p and q, of the form: $\log \Delta m_i^t = p + q\bar{m}_i$ to all the frames, and find $q = 0.3$. This function approximately describes the expected dependence of error on magnitude. Note that, in the case that the background Poisson noise is the dominant source of error, we expect $q = 0.4$, while in the limit of zero background we expect $q = 0.2$. Assuming that $q = 0.3$ is constant over all nights, for each individual frame we refit this formula to obtain p_t. This fit gives, for each frame, the typical error as a function of magnitude. Finally, for each frame, we have compared the χ^2 errors in the magnitudes of the lensed images, *A* and *B* (m_t^A, m_t^B), with the empirical errors $10^{p_t+qm_t^A}$ and $10^{p_t+qm_t^B}$. We find excellent agreement between the two error estimators.

Table 1 lists the reference star coordinates, magnitudes, $\bar{m}_i$, and the 68% confidence interval of their magnitude distribution (68% CI). All magnitudes in this paper are given relative to reference star *S*7.

TABLE 1. PSF REFERENCE STARS

Ref	R.A. (J2000)	Dec.	$\bar{m}_i$	68%CI
*S*1	11:06:33.17	−18:21:39.1	0.262	0.025
*S*2	11:06:33.86	−18:20:29.6	0.585	0.038
*S*3	11:06:44.75	−18:20:43.2	0.374	0.035
*S*4	11:06:38.06	−18:19:10.7	0.344	0.043
*S*5	11:06:30.38	−18:19:33.0	1.633	0.088
*S*6	11:06:29.74	−18:20:02.3	1.321	0.065
*S*7	11:06:23.23	−18:19:41.5	0.000	0.028
*S*8	11:06:22.50	−18:21:30.4	0.384	0.038
*S*9	11:06:35.63	−18:21:29.3	0.987	0.055
*S*10	11:06:37.00	−18:22:45.5	0.414	0.033
*S*11	11:06:37.39	−18:23:00.3	1.551	0.100
*S*12	11:06:38.31	−18:22:48.1	1.284	0.060

NOTE. — Astrometry is based on 38 USNO-A2.0 stars (Monet 1998) with 0.″4 rms in each axis. Magnitudes are given relative to reference star *S*7.

3. WISE-OGLE INTERCALIBRATION

We have intercalibrated the OGLE and Wise photometry, in order to produce combined light curves with a long time coverage. To this end, we take advantage of the fact that the Wise and OGLE light curves overlap in the year 2000 (J.D. ∼ 2451450-2451750). However, the OGLE observations were obtained in the *V* band, while the Wise observations were obtained in the *R* band. Wisotzki et al. (1995) have already noted that the flux ratio between the quasar images depends on wavelength. We therefore intercalibrated the photometry for the light curve of each lensed image separately. For each image, we performed a χ^2 fit between the overlapping OGLE and Wise light curves to determine the magnitude offset and an optional stretch factor. We allow for a stretch factor since quasars are known to vary in color, and the amplitude of variation in the different bands is thus not necessarily the same. We used two types of fits: (i) An offset + stretch factor, $m_R = a + bm_V$, where m_R and m_V are the magnitudes in the *R* and *V* bands, respectively; and (ii) A pure magnitude offset, $m_R = a + m_V$.

Since the OGLE and Wise observations during the overlap period were not carried out on the same days, we linearly interpolated the OGLE observations (which are more frequent and have smaller error bars) to the times of the Wise observations. We set the error of each interpolated magnitude to be

$$\varepsilon = \sqrt{\varepsilon_n^2 + sf(\Delta t_{min})}, \quad (1)$$

where ε_n is the error of the real measurement nearest in time to the interpolated point, $sf(\Delta t_{min})$ is the value of the structure function of the interpolated light curve at lag Δt_{min}, and Δt_{min} is the time between the interpolated epoch and the nearest epoch which has a real measurement. The structure function is defined as

$$sf^2(t) = 2[V - DCF(t)], \quad (2)$$

where V is the variance of the light curve and $DCF(t)$ is the (unnormalized) discrete auto-correlation function (Edelson & Krolik 1988), calculated with 14-day bins. This scheme gives the interpolated points a realistic weight in the χ^2 minimization.

The 1σ errors of the pure magnitude-shift fit between the *V* and *R* light curves are less than 0.03 mag for both images. Applying the shift+stretch fit, the best-fit stretch factor between the *V* and *R* light curves is consistent with unity and does not improve the fit significantly. As we will show below, allowing for a non-unity stretch factor does not change the best fit time delay. Therefore, in what follows we will use the magnitude-shifted light curves (i.e., with no stretch). We test in §4 for the

[1] http://wise-obs.tau.ac.il/∼eran/LM/

[2] The measurements, as well as finding chart with reference stars, are available from http://wise-obs.tau.ac.il/∼eran/LM/HE1104/

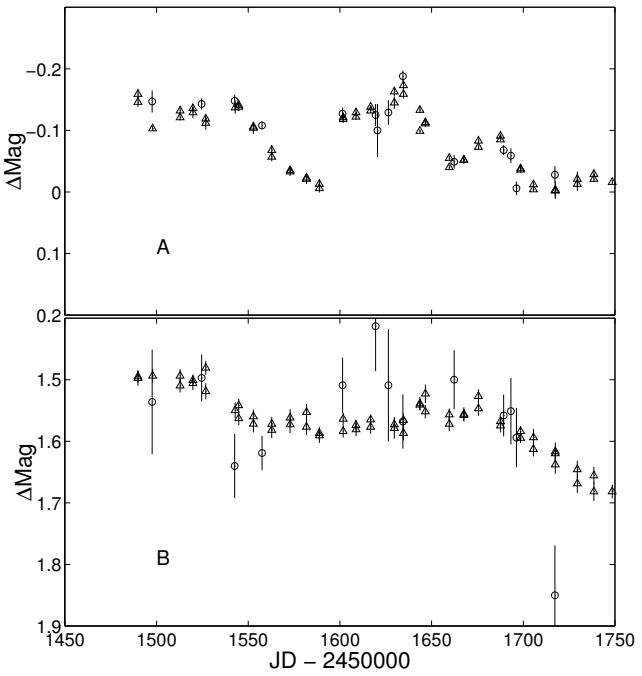

FIG. 1.— Image *A* (upper panel) and image *B* (lower panel) light curves during the period of overlap between the *V*-band OGLE observations (triangles) and the *R*-band Wise observations (circles). The observations were brought to the same scale by χ^2 minimization. Magnitudes are relative to reference star *S*7.

TABLE 2. INTERCALIBRATED IMAGE A LIGHT CURVE

JD-2450000	mag	error	Observatory[a]
666.46490	−0.418	0.005	1
666.47390	−0.418	0.005	1
760.84802	−0.360	0.003	1
760.85665	−0.354	0.003	1
762.85473	−0.341	0.004	1

NOTE. — Table 2a in its entirety, as well as Table 2b for image B, are available via the electronic version.

[a]1- Observations from Schechter et al. (2003; OGLE V band); 2- Our observations (Wise R band).

uncertainty in the time delay induced by the range of possible shift+stretch parameters.

The combined light curves in the zone of overlap are shown in Figure 1, for images *A* (upper panel) and *B* (lower panel). In Figure 2 we show the complete (1997-2002) light curves of images *A* (upper panel) and *B* (lower panel), after application of the intercalibration to the whole dataset. The complete intercalibrated data, from Schechter et al. (2003) and our observations, are given in Table 2.

4. TIME DELAY BETWEEN IMAGES A AND B

We now search for the time delay between images *A* and *B* by using χ^2 minimization. From Figure 2, it is apparent that the long term variation of image *A* is more pronounced than that of image *B*. This could be the result of microlensing in the system. Thus, in the χ^2 minimization we leave as free parameters not only a time delay, but also a linear trend of magnitude with time between the light curves. The fit is described by

$$\chi^2 = \sum_i^N \frac{[m^B_{t+\tau} - m^A_t + S(t - t_{mid}) - C]^2}{\varepsilon_n^2 + sf(\Delta t_{min})} \quad (3)$$

where m^A_t and m^B_t are the magnitudes as a function of the time, t, for images *A* and *B*, respectively. The arbitrary constant t_{mid} is defined as the midpoint between the first and last observations (i.e., $JD = 2451525.378$), C is the mean magnitude difference between the images, and S and τ are the fit parameters – a linear trend between the light curves, and a time delay, respectively. The fit was performed, simultaneously for S and C, between the light curve of image *A* and each of the τ-shifted light curves of image *B*. In this process, the light curve of image *A* at epoch t was interpolated to the times $(t + \tau)$ of the image *B* observations. Again, we used linear interpolation and set the error of the interpolated magnitude using Eq. 1. The bin size used for calculating the DCF necessary for determining the structure function, $sf(\Delta t_{min})$, has a small effect (< 2 days) on the best-fit time delay.

Figure 3 shows the χ^2 per degree of freedom (dof) of the light curve fitting as a function of the time delay. The dashed curve shows the dof. For each time delay, the best-fit linear trend (S) and magnitude offset (C) were recalculated. There is a distinct minimum in the χ^2 at a time delay of -161 day. The best fit parameters are $S = 0.043$ mag yr^{-1} and $\tau = -160.9$ day (with $\chi^2/dof = 303/229 = 1.32$). For these parameters, the magnitude difference (C) between the images in the *R* band is $\Delta m_R = 1.595 \pm 0.004$ mag. Figure 4 shows the light curve of image *A* (filled circles), overlayed by the slope corrected ($S = 0.043$ mag yr^{-1}) and time-delay shifted ($\tau = -160.9$ day) light curve of image *B* (empty circles). The formal χ^2 errors on the time delay are less than 1%. However, these errors are not realistic. As we will show below, there are several sources of systematic errors that need to be taken into account.

As noted above, a systematic error is introduced to the time delay by the uncertainty in the OGLE and Wise intercalibrations (using the shift algorithm or the shift+stretch algorithm). We have used the uncertainty in the shift+stretch parameters and their covariance term, and have run 1000 Monte-Carlo simulations in which we randomly drew shift+stretch parameters from a bivariate Gaussian distribution, and repeated the time-delay fit. We find a time delay distribution of $-159.2^{+0.4,+33}_{-1.7,-2.0}$ day (68% and 95% confidence errors). The short time delays, found in some of these simulations, of about -130 day, are the result of stretch-factor values smaller than $b = 0.75$. Quasars are known to have larger variability amplitudes at bluer wavelengths, corresponding to $b < 1$. For example, Giveon et al. (1999) found $\Delta(B - R) \approx 0.25\Delta B$ for a sample of quasars at $z \sim 0.2$, which corresponds to a stretch factor $b = 0.75$ between *B* and *R*. For HE1104−1805, we are observing a smaller wavelength interval, between *V* and *R*, but on the other hand, a higher redshift. The *V* and *R* bands sample the restframe UV, which may have a stronger dependence of variation amplitude on wavelength. Given the current uncertainty in the stretch factor, there is about 4% probability that the time delay between the images of HE1104−1805 is between -125 and -155 days. If we limit the stretch parameter to $0.75 < b < 1$, then the 95% confidence error on the time delay, due to the stretch + shift uncertainty, is smaller than 2 days.

With these results we can reject the possibility that the time delay is in the region of -250 to -330 days, as suggested

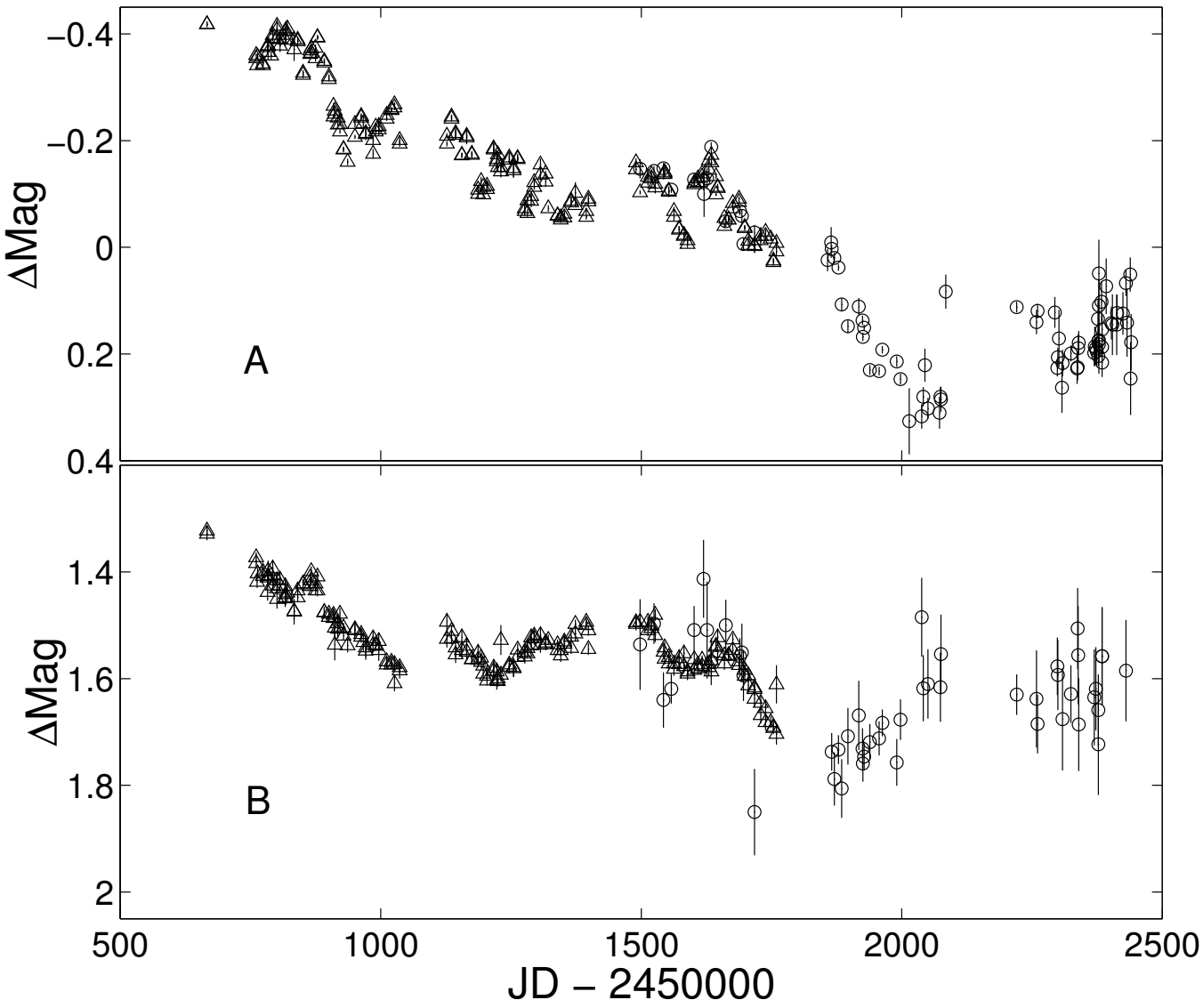

FIG. 2.— Image *A* (upper panel) and image *B* (lower panel) light curves from 1997 to 2002, based on the *V*-band OGLE observations (triangles) and the *R*-band Wise observations (circles), after intercalibration of the two data sets.

by Gil-Merino et al. (2002) and Pelt et al. (2002). Given the significant microlensing variability observed in this system (e.g., Schechter et al. 2003), measuring the time delay from sparsely sampled light curve is difficult.

Figure 4 shows that the main features and trends appear in the light curves of both images. However, there are significant coherent fluctuations in the difference light curve, as already noted by Schechter et al. (2003). Figure 5 shows the difference between the *A* and *B* light curves after applying the best-fit linear trend and time delay. In order to subtract the two light curves we interpolated the time-delay- and linear-trend-corrected light curve of image *B* to the times of image-*A* observations. Note that this plot mixes the *V*- and *R*-band measurements. The error bars were calculated according to:

$$\Delta m = \sqrt{\varepsilon_A^2 + \varepsilon_{Bn}^2 + sf(\Delta t_{min})}, \quad (4)$$

where ε_A is the error for image *A*, and ε_{Bn} is the error for image *B* at the point nearest to the interpolation time. The structure function of the residual light curve, shown in Figure 6, rises rapidly from 0 to 50 days lag (time in the observer system) and then stays approximately constant at a level of 5×10^{-3} mag^2 (≈ 0.07 mag). The structure function was calculated using Eq. 2, where the DCF was calculated with 14 days bins.

The short-timescale, uncorrelated, variability in the light curves is a second source of systematic error in the delay measurement. To evaluate the effect of these fluctuations on the delay accuracy, and to test the hypothesis that the time delay might be completely different (e.g., Gil-Merino et al. 2002), we have performed additional Monte-Carlo simulations. We have used the algorithm of Timmer & Koenig (1995) to artificially generate random red-noise light curves. The light curves were generated with the same temporal sampling pattern as the real observations obtained by OGLE and by us, and with a power density spectrum (PDS) proportional to $f^{-\alpha}$, where f is the frequency and α is the power-law index. The PDS of quasar variability in the optical range is poorly known

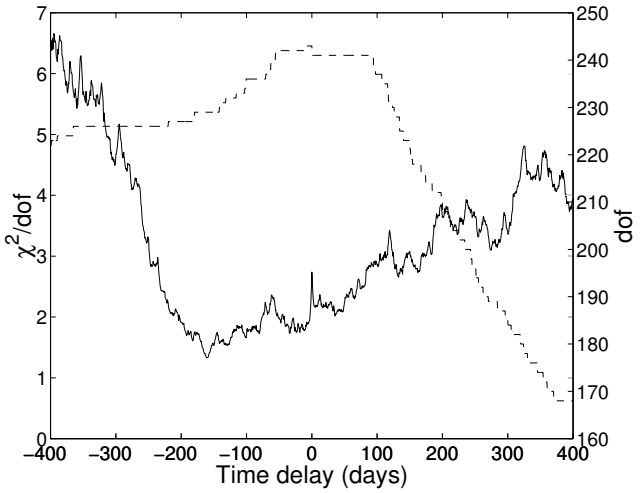

FIG. 3.— The χ^2/dof as a function of delay time (solid curve). For each time delay, the best-fit linear trend (S) and magnitude offset (C) were used. The dashed curve shows the dof.

(see Markowitz et al. 2002, for the PDS in X-rays) but is likely a power law with α between 1 and 2 (Giveon et al. 1999). The standard deviation (StD) of the variations about the mean of the simulated light curve was scaled to the StD of the observed image-B light curve. To simulate the image-A light curve, we duplicated the image-B light curve with a time delay τ_S. We then added to each point in both simulated light curves a normally distributed noise with StD taken from the individual errors in the observed light curves. In order to mimic the uncorrelated noise, we also added, in some of the simulations, the residual light curve (shown in Fig. 5) to the simulated image-A light curve. We then used χ^2 minimization, as for the real data, to search for the best time delay. For each set of parameters (e.g., α, τ_S) we repeated this process 300 times. Note that we do not take into account the linear trend in the simulations.

Our main conclusions from the simulations are: (i) The power-law index α has the largest effect on the uncertainty of the deduced time delay, with a $\sim \pm 1$ day 95%-confidence error for $\alpha = 2$, and a $\sim \pm 7$ day 95%-confidence error for $\alpha = 1$. A small value of α introduces variability on timescales shorter than the mean sampling interval; (ii) When the uncorrelated variability is added to the simulated light curve of image A, the confidence interval increases by about 30%; (iii) Testing for $\tau_s \neq -161$ day (e.g., $\tau_s \approx -300$ day; as suggested by Gil-Merino et al. 2002) gives similar uncertainties in the measured time delay to those found using $\tau_s = -161$ day. Combining the uncertainty from these simulations ($\alpha = 1$), and the systematic errors described above, we have adopted a time delay of $-161^{+7,+34}_{-7,-11}$ day (68% and 95%-confidence errors). Moreover, we can reject with high confidence the possibility that the time delay is in the vicinity of ~ -300 day, as suggested by earlier works on HE1104−1805.

To verify our result using another method, we have applied the ZDCF cross-correlation technique (Alexander 1997) directly to the data. We find a best fit time delay of about -156^{+5}_{-15} day, with a peak correlation of 0.82 ± 0.03, consistent with our χ^2 fit. The result changes by less than 2 days if, before cross-correlating, we subtract the linear trend (S) from the image-A light curve, subtract first degree polynomials from both light curve, or use the image fluxes instead of magnitudes.

5. DISCUSSION AND SUMMARY

We now discuss briefly the implications of the time delay we have found, $\tau = -161 \pm 7$ days. Lehár et al. (2000) modeled the lensing potential of HE1104−1805 using a singular isothermal ellipsoid or a constant mass to light ratio, with and without the external shear expected from galaxies projected within $\sim 20''$, assuming they are at the lens redshift. Their predicted time delays for these four different models are in the range of $-129h^{-1}$ to $-263h^{-1}$ days. Assuming $h = 0.7$ (Bennett et al. 2003), the shortest time delay (-184 days) predicted by the singular isothermal ellipse + external shear model is larger than our result. Note that HE1104−1805 is a double-image lensed quasar, and therefore it was necessary to use the flux ratio between images in order to constrain the lens model. Interestingly, Lehár et al. (2000) note that an external shear twice as large as their most extreme model is needed in order for the lens mass to be aligned with its light. A larger shear would lower the predicted time delay, and make it more consistent with our measurement and with current measurement of H_0. Alternatively, if we adopt the model range of Lehár et al. (2000), our measured limit of $\tau > -172$ day (95% CL) sets a lower limit of $h > 0.75$. HE1104−1805 apparently is an unusual system, as indicated by the fact that the bright image A is the one closer to the lens and that the measured time delay is not consistent with the time delay predicted by simple models. We defer dealing in more detail with the implications of the time delay to a future work.

The mean flux ratio of $A/B \sim 4.4$ we find in this work is significantly different from the emission line flux ratio of $A/B \sim 2.8$ reported by Wisotzki et al. (1993). Extrapolating the linear trend we have found, $S \sim 0.04$ mag yr^{-1}, into the future, suggests that the broad-band flux ratio between the images will decrease to the level of the emission-line flux ratio ($A/B \sim 2.8$) in about a decade. At the source and lens redshifts of HE1104−1805, the Einstein-radius crossing time for stellar objects in the lens galaxy, having mass M and transverse velocity v is $20.3(M/M_\odot)^{1/2}(v/600\mathrm{km\ s^{-1}})^{-1}(h/0.7)^{-1/2}$ yr. Thus, the slow trend is well explained by microlensing in the macro images of HE1104−1805.

As shown in Figures 4 and 5, even after removing a longterm linear trend, there is significant uncorrelated variability. As already noted by Schechter et al. (2003), judging from the amplitude and timescale of the variability, it seems that most of the uncorrelated variability occurs in image A (the one nearest to the lens). Uncorrelated short-timescale variability has been observed in other lensed system (e.g., Burud et al. 2002). However, in HE1104−1805 it has larger amplitudes, with a mean of 0.07 mag (up to 30% peak-to-peak) on timescales of less than a month.

Wambsganss et al. (1990) have pointed out that, for large microlensing optical depth, some events can have timescales that are considerably shorter than the Einstein-radius crossing time. This is caused, for example, by the passage of the source near a cusp. Wyithe & Loeb (2002) have suggested that the low-amplitude, fast ($\sim$ 50 days), uncorrelated variability observed in RXJ0911+05 (Hjorth et al. 2002) and in SBS1520+530 (Burud et al. 2002) can be explained by stellar microlensing of a smooth accretion disk that is occulted by optically thick broad-line clouds. Although their model predicts the short timescale variability, it cannot reproduce the large amplitude observed in HE1104−1805. An-

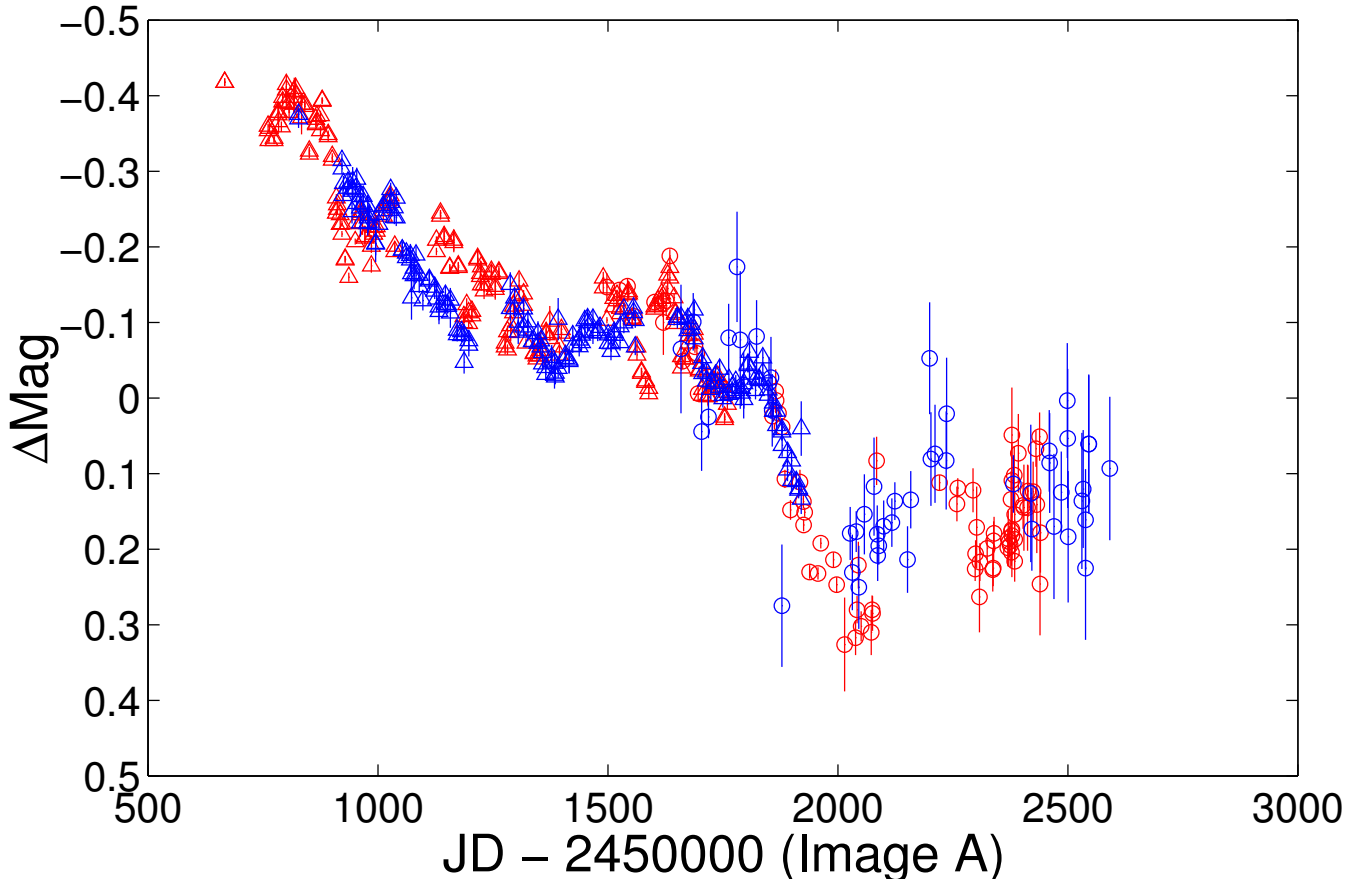

FIG. 4.— Light curve of image *A* (red), overlayed with the best-fitting slope-corrected and time-delay shifted light curve of image *B* (blue). The triangles and circles mark the OGLE and Wise observations, respectively.

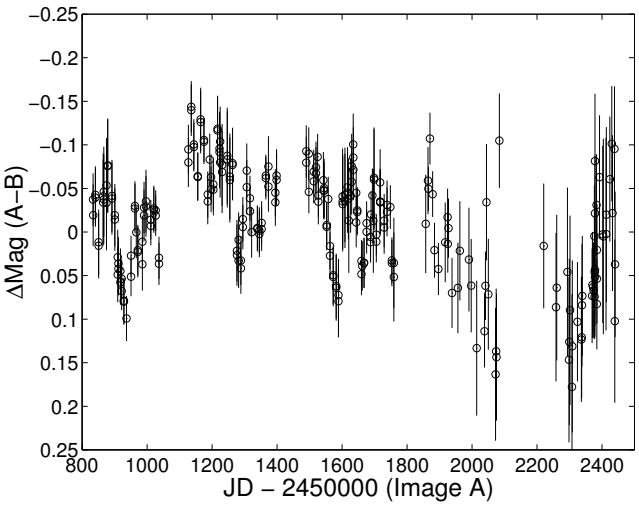

FIG. 5.— The difference light curve between images *A* and *B*, after applying the best-fit linear trend and time delay.

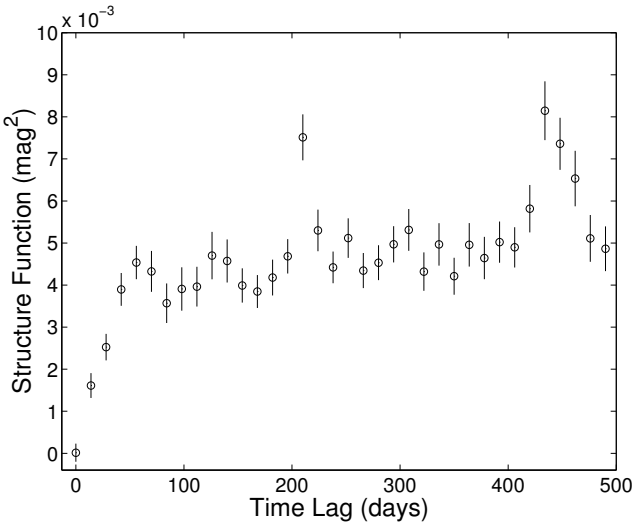

FIG. 6.— Structure function of the difference light curve of Fig. 5.

other possibility they consider is microlensing by planetary-sized objects of $10^{-2} - 10^{-4}$ $M_\odot$, but they show that this cannot produce variations with 10% amplitude or greater. Gould & Miralda-Escude (1997) have suggested that the microlensing of hot spots (or any structure) in the fastly rotating quasar accretion disk can give rise to fast variations with timescales of $\sim$ 1 month. Wyithe & Loeb (2002) have simulated microlensing of an accretion disk with 100 spots. They find a typical variability amplitude of $\sim$ 10% on one-month timescales. Schechter et al. (2003) have argued that the variability in HE1104−1805 is best explained by such a model

with $v/c \sim 0.25$. In order to test these models, we currently continue to observe this system frequently in the *VRI* bands. With more data at hand, we will attempt to re-address the nature of the microlensing in this system in a future paper.

To summarize our main results, we have measured the time delay of the lensed double-image quasar HE1104−1805. We have used detailed simulations at every stage of the reduction and analysis in order to obtain realistic error estimates. We find that the light curves are best fit with a time delay of -161 ± 7 days, and with a linear trend between the images of about ~ 0.04 mag yr^{-1}. Our measurements resolve the previous ambiguities pertaining to the time delay in this system. However, the time delay is shorter than predicted by any existing models. The linear trend is likely due to stellar-mass microlensing in the lens galaxy. We confirm previous reports that the residual light curve between the linear-trend-corrected and time-delay-shifted light curves shows significant variability on short timescales of about one month. Multi-band and spectroscopic observations could help explain the nature of this fast variability.

We thank Paul Schechter, Lutz Wisotzki, Avishay Gal-Yam, Ohad Shemmer, Shay Zucker and Orly Gnat for valuable discussions, and an anonymous referee for an extremely prompt review. This work was supported by a grant from the German Israeli Foundation for Scientific Research and Development.

REFERENCES

Alexander, T. 1997, in: Astronomical Time Series, Eds. D. Maoz, A. Sternberg, and E.M. Leibowitz, 1997 (Dordrecht: Kluwer), p. 163
Bennett, C. L. et al. 2003, ApJ, 583, 1
Burud, I. et al. 2002, A&A, 391, 481
Edelson, R. A. & Krolik, J. H. 1988, ApJ, 333, 646
Gil-Merino, R., Wisotzki, L., & Wambsganss, J. 2002, A&A, 381, 42
Giveon, U., Maoz, D., Kaspi, S., Netzer, H., & Smith, P. S. 1999, MNRAS, 306, 637
Gould, A. & Miralda-Escude, J. 1997, ApJL, 483, L13
Hjorth, J. et al. 2002, ApJL, 572, L11
Kochanek, C. S. 2002, ApJ, 578, 25
Lehár, J. et al. 2000, ApJ, 536, 584
Lidman, C., Courbin, F., Kneib, J.-P., Golse, G., Castander, F., & Soucail, G. 2000, A&A, 364, L62
Markowitz, A. et al. 2003, ApJ, in press, astro-ph/0303273
Monet, D., et al. 1998 USNO-A2.0, (U.S. Naval Observatory, Washington DC).
Pelt, J., Refsdal, S., & Stabell, R. 2002, A&A, 389, L57
Press, W. H., Teukolsky, S. A., Vetterling, W. T., & Flannery, B. P. 1992, Cambridge: University Press, —c1992, 2nd ed.,
Schechter, P. L. & Wambsganss, J. 2002, ApJ, 580, 685
Schechter, P. L. et al. 2003, ApJ, 584, 657
Timmer, J. & Koenig, M. 1995, A&A, 300, 707
Turner, E. L., Cen, R., & Ostriker, J. P. 1992, AJ, 103, 1427
Wambsganss, J., Paczynski, B., & Schneider, P. 1990, ApJL, 358, L33
Wambsganss, J. 2002, in Active Galactic Nuclei: from Central Engine to Host Galaxy, Eds.: S. Collin, F. Combes and I. Shlosman (San-Francisco: PASP), p. 17
Williams, L. L. R. & Saha, P. 2000, AJ, 119, 439
Wisotzki, L., Koehler, T., Kayser, R., & Reimers, D. 1993, A&A, 278, L15
Wisotzki, L., Koehler, T., Ikonomou, M., & Reimers, D. 1995, A&A, 297, L59
Wisotzki, L., Wucknitz, O., Lopez, S., & Sorensen, A. N. 1998, A&A, 339, L73
Wyithe, J. S. B., Agol, E., & Fluke, C. J. 2002, MNRAS, 331, 1041
Wyithe, J. S. B. & Loeb, A. 2002, ApJ, 577, 615